SCIENTIFIC REPORTS

OPEN

SUBJECT AREAS:
ELECTRONIC DEVICES
TWO-DIMENSIONAL MATERIALS
ELECTRONIC PROPERTIES AND MATERIALS
ELECTRONIC MATERIALS

Received
25 February 2013

Accepted
17 May 2013

Published
3 June 2013

Correspondence and requests for materials should be addressed to Y.X. (yxie@ustc.edu.cn)

High-performance flexible electrochromic device based on facile semiconductor-to-metal transition realized by $WO_3 \cdot 2H_2O$ ultrathin nanosheets

Lin Liang, Jiajia Zhang, Yingying Zhou, Junfeng Xie, Xiaodong Zhang, Meili Guan, Bicai Pan & Yi Xie

Hefei National Laboratory for Physical Sciences at the Microscale, University of Science & Technology of China, Hefei, Anhui, 230026, P.R. China.

Ultrathin nanosheets are considered as one kind of the most promising candidates for the fabrication of flexible electrochromic devices (ECDs) due to their permeable channels, high specific surface areas, and good contact with the substrate. Herein, we first report the synthesis of large-area nanosheets of tungsten oxide dihydrate ($WO_3 \cdot 2H_2O$) with a thickness of only about 1.4 nm, showing much higher Li^+ diffusion coefficients than those of the bulk counterpart. The $WO_3 \cdot 2H_2O$ ultrathin nanosheets are successfully assembled into the electrode of flexible electrochromic device, which exhibits wide optical modulation, fast color-switching speed, high coloration efficiency, good cyclic stability and excellent flexibility. Moreover, the electrochromic mechanism of $WO_3 \cdot 2H_2O$ is further investigated by first-principle density functional theory (DFT) calculations, in which the relationship between structural features of ultrathin nanosheets and coloration/bleaching response speed is revealed.

Electrochromic (EC) materials, which can reversibly change their optical properties (reflectance, transmittance, and absorbance) under applied voltage, are one kind of the most important branches of chromic materials[1–3]. In the past few years, electrochromic devices (ECDs) made of these materials have attracted tremendous attention due to their potential applications, such as smart windows, optical displays and rear-view mirrors[4–6]. Besides rigid ECDs fabricated using glass substrates, flexible electrochromic devices have gradually become an important demand, since such devices could achieve "retrofit" installation on existing structures and reduce production costs compared to new installation[7–9]. However, the development and practical application of flexible ECDs are seriously restricted by the fabrication techniques and electrochromic materials. Traditional techniques for fabricating flexible electrochromic films include magnetron sputtering, plasma-enhanced chemical vapor deposition, electrodeposition and lithography, which usually require expensive equipments, rigorous experimental conditions and multiple processing steps[10–12]. Bulk or nanosized particles, as the conventional candidates for electrochromic materials, are liable to crack and detach from the substrate after repetitive bending or strain, owing to poor adhesion between materials and flexible substrate[13,14]. In addition, the nanoparticles tend to aggregate and form large secondary particles because of the van der Waals attraction, which largely reduces the contact areas of active materials and electrolyte and hinders ion diffusion in electrochromic layer[15]. Therefore, it is a great challenge for scientists to synthesize novel electrochromic materials and develop new fabrication techniques for flexible ECDs with enhanced performance.

As is rapidly emerging recently, two-dimensional (2D) nanosheets are the most promising building blocks for the design of ultrathin, transparent, and flexible paperlike devices[16,17]. These 2D nanosheets could provide the bridge to effectively connect microscopic and macroscopic processes, guaranteeing a maximum functionality while keeping the size minimized[16,18]. As a typical example, the one-atomic-thick carbon nanosheet, graphene, has been widely applied in transparent conducting electrodes, supercapacitors, field-effect transistors, and so on[19–21]. Besides graphene, other 2D nanosheets of various materials, including transition-metal chalcogenides, metal oxides and hydroxides, have recently sparked worldwide interests owing to their unique electronic structures and

physical properties compared with the corresponding bulk samples[22–24]. As is well known, electrochromic performance mainly relies on the diffusion of ions in the electrochromic material. Ultrathin nanosheets with open 2D permeable channels could maximize the utilization ratio of the active materials and reduce diffusion paths of the ions significantly, resulting in faster color-switching speed and higher coloration efficiency. Moreover, the 2D configuration with large surface area allows for high interfacial contact area with the electrolyte and intimate contact with the substrate, thus facilitating fast interfacial charge transfer and enhancing flexibility of the devices. In a word, ultrathin 2D nanosheets could provide an ideal platform for fabricating flexible electrochromic devices.

Over the past few decades, a series of tungsten oxides have been extensively investigated due to their high coloration efficiency and good cyclic stability among various electrochromic materials[25–27]. Besides anhydrous tungsten oxide, several tungsten oxide hydrates have gradually attracted more attention, such as $WO_3 \cdot 2H_2O$ (dihydrate), $WO_3 \cdot H_2O$ (monohydrate), $WO_3 \cdot 0.5H_2O$ (hemihydrate) and $WO_3 \cdot 0.33H_2O$[28–32]. Judeinstein and Marcel have reported that water has a beneficial effect on lithium insertion kinetics into tungsten oxide[33,34]. Thus, we think that tungsten oxide dihydrate ($WO_3 \cdot 2H_2O$) may be a promising candidate applied for electrochromic materials. However, $WO_3 \cdot 2H_2O$ has been neglected for a long time, and never been utilized in flexible ECDs. As far as we know, $WO_3 \cdot 2H_2O$ possesses a layered structure, which is made of distorted $WO_5(H_2O)$ octahedrons in corner sharing mode. The $WO_5(H_2O)$ octahedrons are connected with each other to form a $WO_3[H_2O]$ layer. The other half of water is located between such layers as interlayer water[29,35]. The existence of interlaminar water can increase the distance between adjacent layers to supply a larger spacing, facilitating ionic intercalation/deintercalation during electrochromic process[36,37]. Moreover, the interlayer spacing of $WO_3 \cdot 2H_2O$ is larger than other tungsten oxide hydrates, which makes $WO_3 \cdot 2H_2O$ facilely exfoliate into 2D nanosheets.

Herein, we put forward a novel and convenient strategy to synthesize tungsten oxide dihydrate ultrathin nanosheets as the electrode material of the flexible electrochromic device. In this strategy, lamellar inorganic-organic hybrid intermediate is firstly prepared by the insertion of dodecylamine into the interlamination of tungstic acid, and then is easily exfoliated in nitric acid solution to form $WO_3 \cdot 2H_2O$ nanosheets with a thickness of only about 1.4 nm. The obtained ultrathin nanosheets can be assembled into large-area films using the convenient filtration technique, and then the as-assembled film with outstanding structural integrity can easily transfer into a flexible substrate for fabricating flexible electrochromic device. The obtained device displays wide optical modulation, fast coloration/bleaching response speed, high coloration efficiency, good cycling stability and excellent flexibility. In addition, we further study the electrochromic mechanism of $WO_3 \cdot 2H_2O$ and explain the relationship between the structural feature of ultrathin nanosheets and color-switching speed.

Results

In this study, tungsten oxide dihydrate ultrathin nanosheets were successfully synthesized via ultrasonic exfoliation of inorganic-organic hybrid intermediate. The intermediate was firstly prepared by a convenient reaction between tungstic acid (H_2WO_4) and dodecylamine ($C_{12}H_{25}NH_2$) in heptane. The X-ray powder diffraction (XRD) patterns of the obtained intermediate are shown in **Figure S1**, from which the diffraction peaks belonging to H_2WO_4 disappear and a series of new diffraction peaks in the low-angle regions occur. These peaks can be indexed to the (00l) reflections (l = 1,2,3, …), which indicates that tungstate-based inorganic-organic nanohybrids possess a well-ordered lamellar microstructure. The interlayer spacing of the sample is calculated to be 3.4 nm according to (00l) reflections in the XRD patterns.

When lamellar inorganic-organic hybrid intermediate was reacted with nitric acid solution, a color change from white to light yellow was obviously observed. After centrifugation to remove the nonexfoliated component, the supernatant of $WO_3 \cdot 2H_2O$ ultrathin nanosheets was obtained. As shown in **Figure 1a**, the XRD pattern of $WO_3 \cdot 2H_2O$ ultrathin nanosheets-based film fabricated by a layer-by-layer assembly strategy, can be readily indexed to be monoclinic $WO_3 \cdot 2H_2O$ (JCPDS Card No.18-1420) and displays a highly (010) preferred orientation[35]. This not only reveals the high orientation of the $WO_3 \cdot 2H_2O$ ultrathin nanosheets-based film, but also illustrates that the nanosheet has a (010) preferred orientation, which is further verified by the corresponding high-resolution transmission electron microscopy (HRTEM) image and the selected-area electron diffraction (SAED) pattern in **Figure 1c**. The transmission electron microscopy (TEM) image of the exfoliated product depicted in **Figure 1d** clearly shows a large-area 2D nanosheet with lateral size larger than 500 nm, while the nearly transparent feature indicates the ultrathin thickness. Macroscopically, the colloidal suspension of the exfoliated product is highly stable over several days and displays Tyndall phenomenon (inset in **Figure 1d**), reasonably inferring the formation of stable and homogeneous $WO_3 \cdot 2H_2O$ ultrathin nanosheets[38]. Moreover, as shown in **Figure 1(e–g)**, the atomic force microscopy (AFM) image, the corresponding height distribution and height profiles display the large sheet-like morphology with a height of about 1.4 nm, which corresponds to twice the interlayer distance of 0.696 nm between adjacent $WO_3[H_2O]$ layers along the [010] direction (**Figure 1b**). Therefore, all the above mentioned results unambiguously show that we develop a convenient strategy to obtain large-area $WO_3 \cdot 2H_2O$ nanosheets with a thickness of only about 1.4 nm, providing the prerequisites for their application in the construction of flexible electronic devices.

Based on the above experimental results, a possible formation process of $WO_3 \cdot 2H_2O$ ultrathin nanosheets is suggested as follows. First, in a nonpolar medium of heptane, dodecylamine molecules are intercalated into the interlamination of adjacent $WO_3[H_2O]$ layers in H_2WO_4, leading to the production of lamellar hybrid intermediate. Then, the obtained lamellar intermediate is reacted with nitric acid solution, and the organic species within the interlayers are removed and topotactically replaced by water molecules[39]. Simultaneously, under stirring and ultrasonication, the lamellar hybrid intermediate is exfoliated to form $WO_3 \cdot 2H_2O$ ultrathin nanosheets. The large interlayer spacing of the lamellar intermediate plays an important role in the exfoliation process, which strongly facilitates the formation of ultrathin nanosheets. The whole formation mechanism of $WO_3 \cdot 2H_2O$ ultrathin nanosheets is proposed as illustrated in **Figure 2**.

To fabricate flexible electrode for electrochromic device, the suspension of the as-exfoliated $WO_3 \cdot 2H_2O$ ultrathin nanosheets was vacuum filtrated over a cellulose membrane to form a free-standing homogeneous thin film. The layer-by-layer reassembly process can reinforce the attachment between individual ultrathin nanosheets, and this intimate attachment is very crucial to enhance the electrochromic performance due to the fast charge transfer through tightly stacked nanosheets. Furthermore, the thickness and size of the flexible thin film can be facilely adjusted by varying the concentration of the suspension and the size of the membrane, respectively. Then the thin film was easily transferred onto an indium tin oxide (ITO)-coated polyethylene terephthalate (PET) sheet as a working electrode for our flexible ECD. Considering the requirement of transparency in the device, naked ITO/PET sheet was selected as a flexible counter electrode. Owing to the rapid dissolution of ITO/PET in acidic electrolyte, 1 M solution of lithium perchlorate in propylene carbonate was prepared as the electrolyte. The flexible electrochromic device (designated as nanosheets-based ECD) was assembled as shown in **Figure 3a**, and the ITO layers of working electrode and counter electrode used as current collectors were connected to the

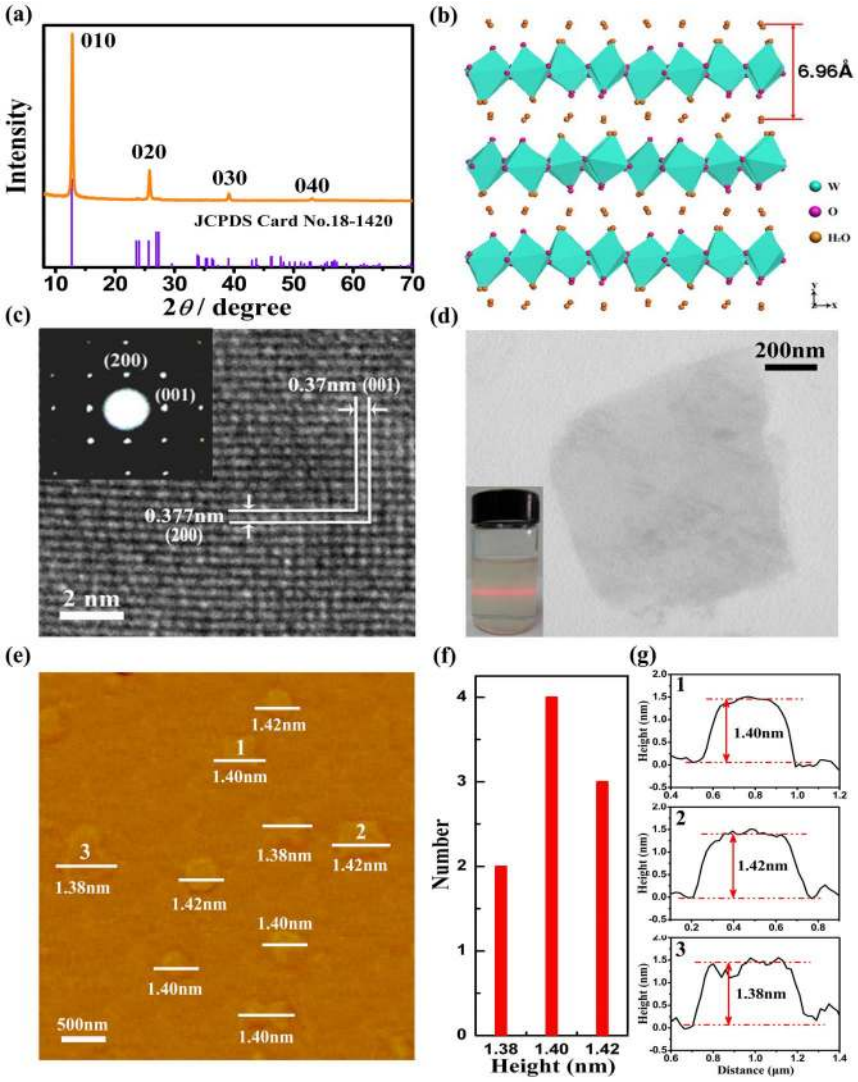

Figure 1 | Characterization of as-obtained $WO_3 \cdot 2H_2O$ ultrathin nanosheets. (a) XRD pattern of $WO_3 \cdot 2H_2O$ ultrathin nanosheets-based film fabricated by a layer-by-layer assembly strategy, the violet lines give the corresponding standard pattern of JCPDS Card No.18-1420. (b) Crystal structure of monoclinic $WO_3 \cdot 2H_2O$ giving the interlayer spacing of 6.96 Å. (c) HRTEM image of $WO_3 \cdot 2H_2O$ ultrathin nanosheet and the corresponding SAED pattern (inset). (d) TEM image of $WO_3 \cdot 2H_2O$ ultrathin nanosheet and the corresponding colloidal dispersion displaying the Tyndall effect (inset). (e) AFM image of $WO_3 \cdot 2H_2O$ ultrathin nanosheets. (f) The corresponding height distribution. (g) Height profiles, the numbers from 1 to 3 in g correspond to the numbers from 1 to 3 in e.

electrochemical test equipment. Notably, the fabrication process of the whole ECD is easy, low-cost and operable, which effectively avoid the problems of traditional techniques as mentioned in the introduction. Furthermore, the obtained ECD is extremely flexible, which is an essential feature for the utilization in flexible electronics. For comparison, the electrochromic device made of $WO_3 \cdot 2H_2O$ bulk powder was also fabricated and designated as bulk-based ECD (for details see experimental section).

Figure 3b shows the optical transmittance spectra and the corresponding photographs of electrochromic device fabricated from $WO_3 \cdot 2H_2O$ ultrathin nanosheets under applied potentials of 3 V and −3 V, respectively. The color of the ECD can switch between colorless (bleached state) and deep blue (colored state) with the electric potential variation. From the transmittance spectra, it can be seen that the optical transmittance of ultrathin nanosheets-based ECD is 69% in the bleached state (3 V) and 21% in the colored state (−3 V) at a wavelength of 798 nm. The transmittance variation of nanosheets-based ECD reaches about 48%, which is much higher than 16.2% of the comparative bulk-based ECD (**Figure S2**). The transmittance of bleached nanosheets-based ECD is 72% at a wavelength of 1300 nm, and when a coloration potential is applied, the transmittance is reduced to about 5%. The optical modulation of nanosheets-based ECD in the wavelength region above 800 nm is very important, as thermal energy radiated in the IR region falls into this range[40]. The distinct optical modulation of over 65% in the near IR region indicates that $WO_3 \cdot 2H_2O$ ultrathin nanosheet is an ideal infrared switch material for the potential application in smart window.

To investigate the color-switching time of the ECDs, the corresponding in situ coloration/bleaching transmittance response was measured at a wavelength of 700 nm with alternately applying potential of ± 3.0 V for 30 s (**Figure 3c**). The color-switching time is defined as the time to reach 90% of the final change in transmittance between the steady bleached and colored states. For nanosheets-based ECD, the color-switching time is 5.1 s from the bleached state to the colored state and 9.7 s for the reverse process, which is faster than those of the bulk-based ECD. The latter ECD takes longer coloration/bleaching time of 13.4 s and 12.5 s, respectively. It is noteworthy that the coloration time of nanosheets-based ECD reduces to 5.1 s, which is quite an outstanding value

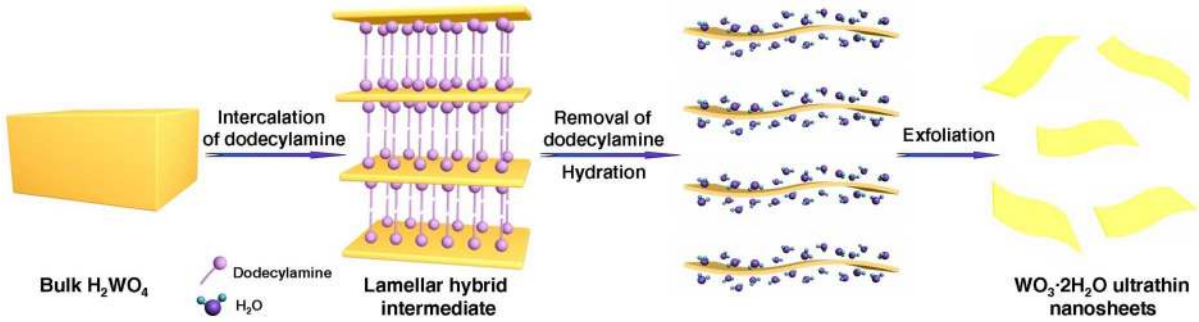

Figure 2 | **Schematic illustration of the formation mechanism of $WO_3{\cdot}2H_2O$ ultrathin nanosheets.**

for tungsten oxide based ECDs in light of previous reports (typically > 10 s)[26,30,41–45].

As is well known, the electrochromism of $WO_3{\cdot}2H_2O$ is due to the intercalation of Li^+ and electrons during the cathodic scan to form $Li_xWO_3{\cdot}2H_2O$ (blue) and their expulsion in the reverse scan to yield $WO_3{\cdot}2H_2O$ in a bleached state (colorless)[43]. Undoubtedly, the intercalation and deintercalation of Li^+ would inevitably influence the electronic structure of materials[46]. To explore the variation of electronic structure deriving from Li^+ intercalation, we carried out first-principle density functional theory (DFT) calculations for $WO_3{\cdot}2H_2O$ ultrathin nanosheets. As shown in **Figure 4a**, the Fermi level positioned within the forbidden energy gap is consistent with its semiconductor feature[46,47]. It is found that the valence and conduction bands are mainly dominated by the O 2p and W 5d orbitals, respectively. When applied with a small voltage on $WO_3{\cdot}2H_2O$, lithium ions and electrons are inserted into $WO_3{\cdot}2H_2O$ EC layer, resulting in the formation of $Li_xWO_3{\cdot}2H_2O$ ultrathin nanosheet. As can be seen from the crystal structure of $WO_3{\cdot}2H_2O$, there are two potential sites for Li^+ intercalation. One is placed between the interlamination of $WO_3[H_2O]$ layer, while the other is located within the distorted $WO_5(H_2O)$ octahedrons. Considering the influence of Li^+ position on the electronic structure, the DFT calculations for $Li_xWO_3{\cdot}2H_2O$ ultrathin nanosheets with two intercalation sites are performed, respectively. As shown in **Figure 4b and 4c**, calculation results reveal that the position of Li^+ has negligible influence on the electronic structure of $Li_xWO_3{\cdot}2H_2O$. Significantly, the Fermi level of $Li_xWO_3{\cdot}2H_2O$ ultrathin nanosheets is shifted into the conduction band, revealing a metallic state. The Li 2s orbital is located above the Fermi level, which implies that lithium is fully ionized in the oxide and the charge-balancing electron occupies the bottom of the conduction band[46–48]. The calculations above strikingly indicate that $WO_3{\cdot}2H_2O$ ultrathin nanosheets show a transition from semiconducting to metallic state accompanied by Li^+ intercalation. For the bulk counterpart, we find the similar transition characteristic in the light of the DFT calculations for bulk $WO_3{\cdot}2H_2O$ and $Li_xWO_3{\cdot}2H_2O$ (**Figure S3**). According to the previous reports, the semiconductor-to-metal transition will lead to the modulation of optical properties and indeed is the reason of the electrochromism[47–49].

As shown in **Figure 5a**, the coloration/bleaching response time depends on the rates of reversible transition between $WO_3{\cdot}2H_2O$ and $Li_xWO_3{\cdot}2H_2O$, which are controlled by the rates of diffusion for Li^+ intercalation/deintercalation[46,49]. For the coloration process, it is very difficult for transferring of Li^+ in the bulk-based ECD, owing to small contact areas between $WO_3{\cdot}2H_2O$ bulk samples and electrolyte and the high resistance from semiconducting ($WO_3{\cdot}2H_2O$) to metallic state ($Li_xWO_3{\cdot}2H_2O$)[50]. However, benefiting from the structural features of ultrathin nanosheets, such as large specific surface areas and good contact with the substrate, the Li^+ diffusion coefficient and the coloration speed of nanosheets-based ECD will be expected improved owing to the reducing diffusion paths of ions and the increasing utilization ratio of the active materials. Therefore, the coloration time of nanosheets-based ECD is 5.1 s, which is faster than that of the bulk-based ECD (13.4 s). Since the bleaching process corresponds to the transition from metallic state to semiconductor, the electrochromic layer will be conductive to the diffusion of Li^+ whether it is composed of ultrathin nanosheets or not. Nevertheless, the interaction force between Li^+ and $WO_3{\cdot}2H_2O$ crystal structure, makes Li^+ transfer with difficulty from electrochromic materials to electrolyte, resulting that the bleaching response is decelerated[47,48,51]. Since ultrathin nanosheets with open 2D permeable channels could effectively increase the contact areas between active materials and electrolyte and promote Li^+ diffusion, the bleaching time of nanosheets-based ECD (9.7 s) is a little faster than that of bulk-based ECD (12.5 s). The experimental data indicate only modest variation in color-switching time between ultrathin nanosheets and bulk counterpart, but the coloration/bleaching response speed for nanosheets-based ECD shows notable improvement compared to the bulk-based ECD. The reason is that the response speed is not an isolated characteristic, which correlates with both transmittance variation and color-switching time as shown in **Figure 3c**. Theoretically, the larger transmittance variation will take longer color-switching time at the same switching speed. For nanosheets-based ECD, the color-switching time is 5.1 s from the bleached state to the colored state and 9.7 s for the reverse process, in which the transmittance variation reaches about 41.7%. For the comparative bulk-based ECD, the coloration time and the bleaching time are 13.4 s and 12.5 s, respectively. However, the electrochromic process of the bulk-based ECD corresponds to small transmittance variation, which is only 9.4%. Therefore, $WO_3{\cdot}2H_2O$ ultrathin nanosheets can facilitate the semiconductor-to-metal transition and notablely enhance the coloration/bleaching response speed, especially for the coloration process.

To further evaluate the Li^+ diffusion coefficient in the $WO_3{\cdot}2H_2O$ ultrathin nanosheets and bulk powder, cyclic voltammograms of ultrathin nanosheets and bulk powder films deposited on ITO glasses were carried out with different potential scan rates as shown in **Figure 5b and 5c**, respectively[43,50,52]. When the peak currents are plotted against the square root of scan rates, $v^{1/2}$, approximately a linear relationship is obtained (insets of **Figure 5b and 5c**), which signifies a diffusion-controlled process. The Li^+ diffusion coefficient can be calculated from a linear relationship between i_p and $v^{1/2}$ according to the following equation,

$$i_p = 2.69 \times 10^5 n^{3/2} A D^{1/2} C v^{1/2} \quad (1)$$

here n is the number of electrons and assumed to be 1, i_p is the peak current (A), D is the diffusion coefficient of Li^+ ($cm^2\ S^{-1}$), A is the electrode area (cm^2), C is the concentration of active ion (Li^+) (mol cm^{-3}), and v is the potential scan rate ($V\ s^{-1}$). According to the above equation, the Li^+ diffusion coefficients in $WO_3{\cdot}2H_2O$ ultrathin

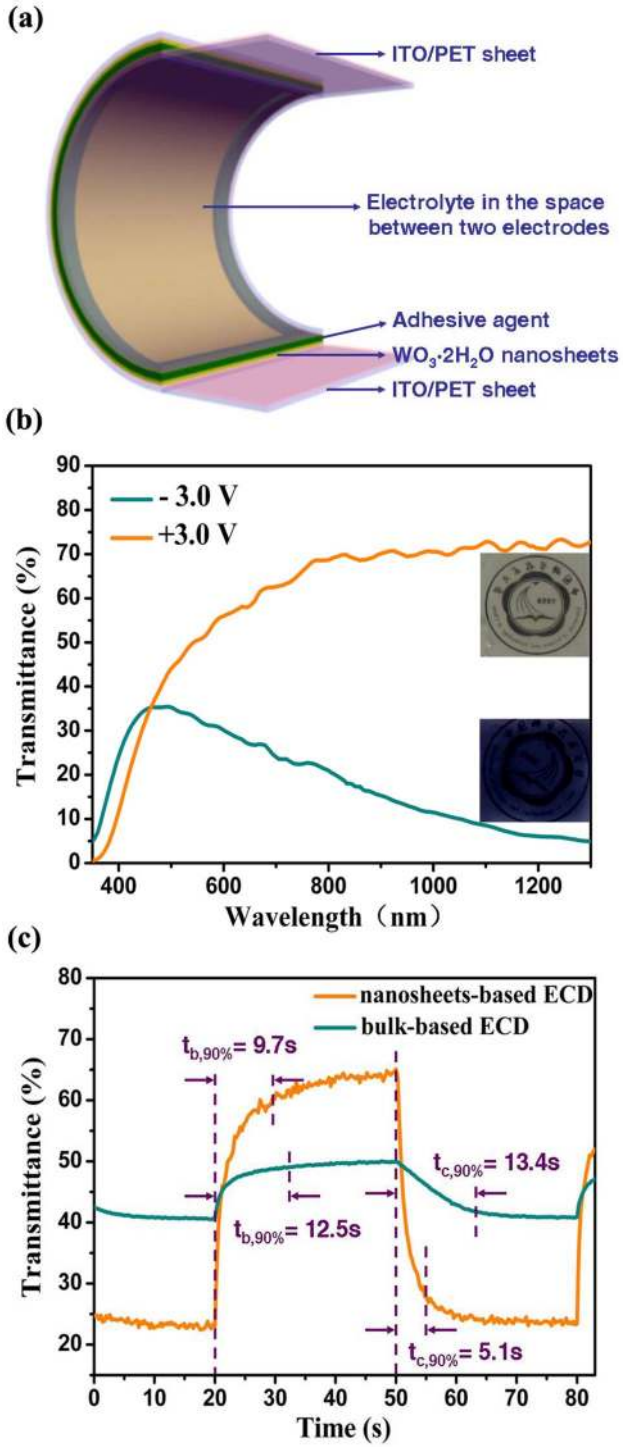

Figure 3 | Setup and electrochromic performances of $WO_3 \cdot 2H_2O$ nanosheets-based flexible electrochromic device. (a) Schematic illustration of the flexible electrochromic device. (b) Optical transmittance spectra and photographs of $WO_3 \cdot 2H_2O$ nanosheets-based ECD under potentials of +3 V and −3 V, respectively. (c) Transmittance variation and switching time characteristics between the colored and bleached states for both the $WO_3 \cdot 2H_2O$ nanosheets-based ECD and the comparative bulk-based ECD measured at ± 3.0 V for 30 s with a wavelength of 700 nm.

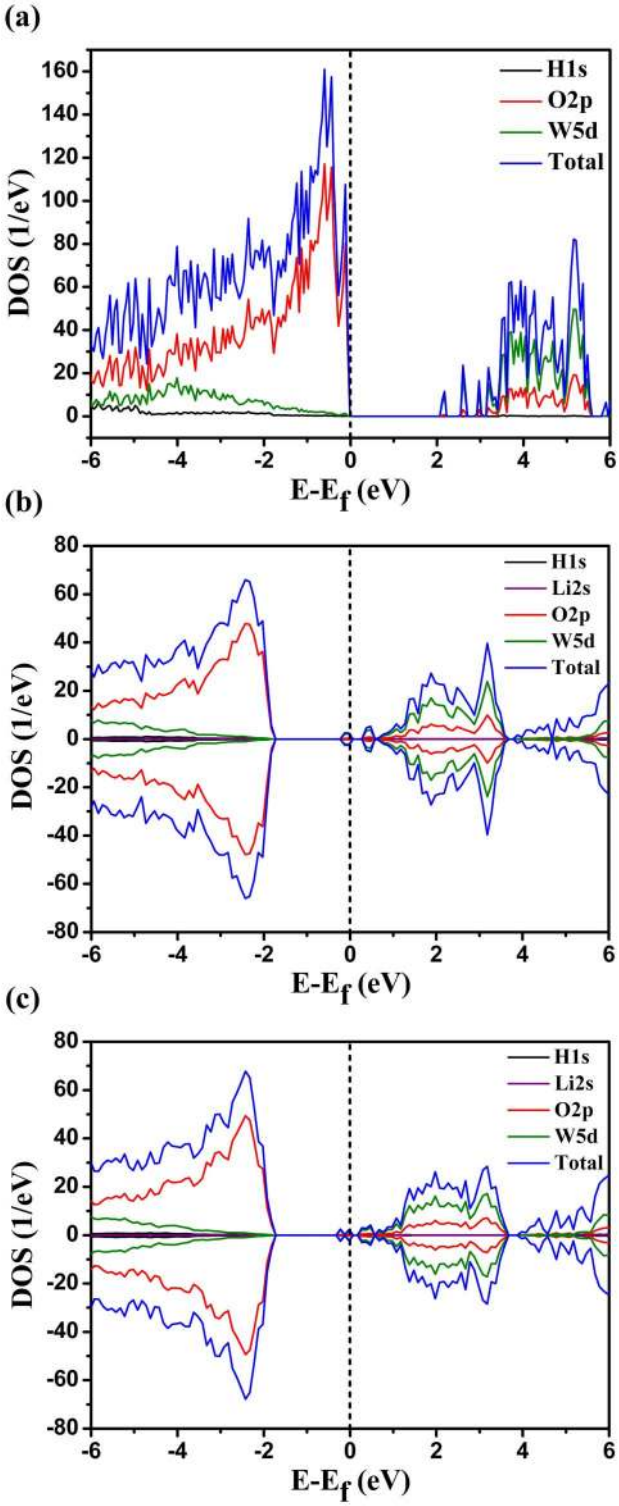

Figure 4 | Density functional theory (DFT) calculations for $WO_3 \cdot 2H_2O$ ultrathin nanosheets before and after Li^+ intercalation. (a) Calculated densities of states for $WO_3 \cdot 2H_2O$ ultrathin nanosheets. Calculated densities of states for $Li_xWO_3 \cdot 2H_2O$ ultrathin nanosheets with two potential sites for Li^+ intercalation: (b) between the interlamination of $WO_3[H_2O]$ layer; (c) within the distorted $WO_5(H_2O)$ octahedrons.

nanosheets are calculated to be 6.19×10^{-10} and 1.23×10^{-10} cm^2 S^{-1} for the intercalation and deintercalation process, respectively. For the $WO_3 \cdot 2H_2O$ bulk powder, the calculated Li^+ diffusion coefficients are 7.5×10^{-11} and 1.2×10^{-11} cm^2 S^{-1} for the intercalation and deintercalation process, respectively. As is expected, the Li^+ diffusion coefficients of $WO_3 \cdot 2H_2O$ ultrathin nanosheets are much higher than those of $WO_3 \cdot 2H_2O$ bulk powder, in accordance with the above discussion.

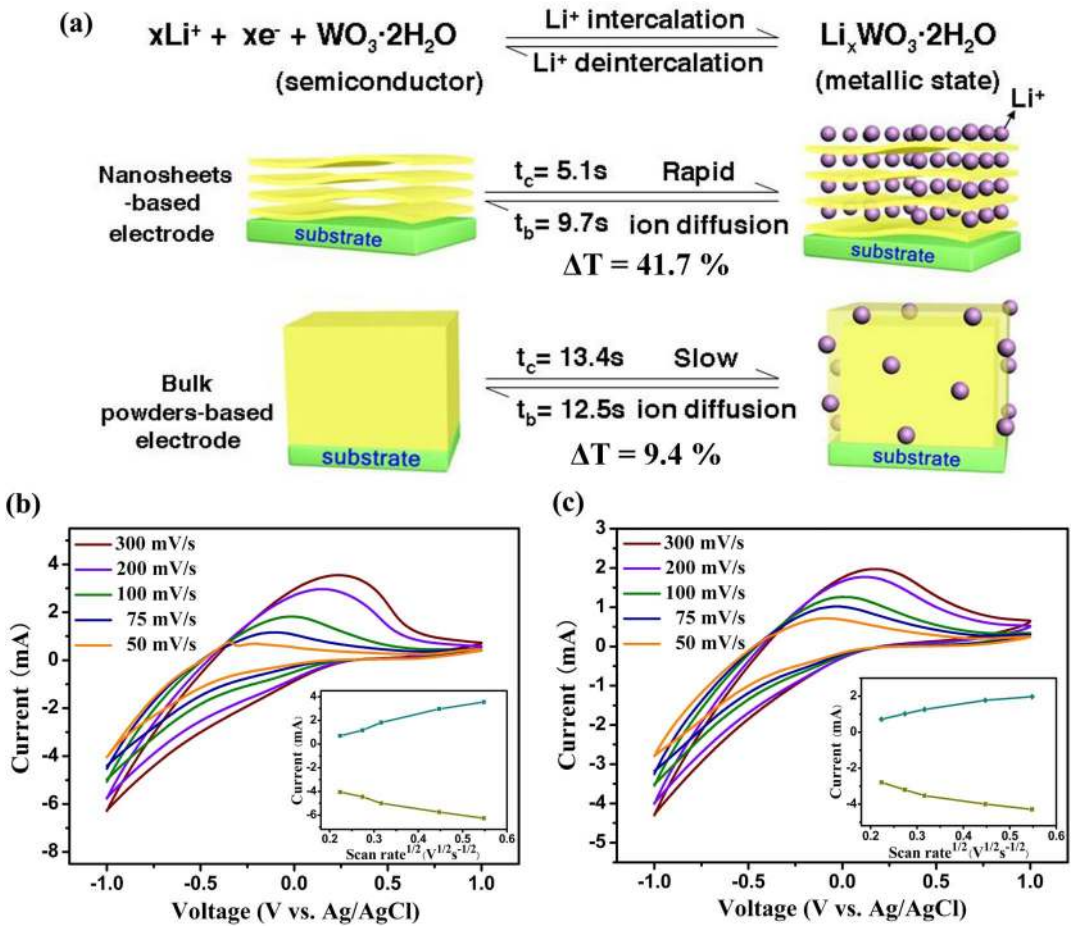

Figure 5 | The comparison of color-switching speed and cyclic voltammograms for $WO_3 \cdot 2H_2O$ with different morphologies. (a) Schematic illustration of the relationship between the morphology of electrochromic materials and coloration/bleaching response speed. Cyclic voltammograms of $WO_3 \cdot 2H_2O$ (b) ultrathin nanosheets and (c) bulk powder. The scan rates are 50 mV s^{-1}, 75 mV s^{-1}, 100 mV s^{-1}, 200 mV s^{-1} and 300 mV s^{-1}, respectively. The insets show the cathodic/anodic peak current as a function of the square root of the scan rates for $WO_3 \cdot 2H_2O$ (b) ultrathin nanosheets and (c) bulk powder.

Another important criterion for identifying the electrochemical performance of ECDs is the coloration efficiency (CE), which represents the change in the optical density (OD) per unit charge density (Q/A, which is the change of the charge (Q) consumed per unit electrode area (A)) during switching. It can be calculated according to the following formulas:

$$CE = \Delta(OD)/\Delta Q \quad (2)$$

$$OD = \log(T_b/T_c) \quad (3)$$

here T_b and T_c refer to the bleached and colored transmittance at a certain wavelength, respectively. **Figure 6a** shows plots of the in situ optical density at a wavelength of 700 nm versus inserted charge density at a coloration potential of −3.0 V. The CE value is extracted as the slope of the line fitted to the linear region of the curve. The calculated CE value of $WO_3 \cdot 2H_2O$ nanosheets-based ECD is 120.9 cm^2 C^{-1}, which is much higher than that of bulk-based ECD (38.5 cm^2 C^{-1}). The higher CE value indicates that $WO_3 \cdot 2H_2O$ nanosheets-based ECD can provide large optical modulation with small changes in insertion or extraction quantities. This is a crucial parameter for practical devices, since a lower charge-insertion or -extraction rate enhances the cyclic stability.

Furthermore, the long-term cycling stability of $WO_3 \cdot 2H_2O$ nanosheets-based ECD was also investigated. **Figure 6b** shows the coloration/bleaching transmittance response curves of the device for the first and 400th cycles, at a wavelength of 700 nm by applying a square-waved voltage (between −3.0 and 3.0 V, each state for 30 s). The nanosheets-based ECD retains the electrochromic properties after 400 switching cycles, with little changes of optical contrast and switching time. To study the flexibility of the device, the coloration/bleaching transmittance response under bending configuration was also researched. As shown in the green line of Figure 3d, under bending configuration, the transmittance response curve of $WO_3 \cdot 2H_2O$ nanosheets-based ECD after 400 cycles does not exhibit obvious changes compared with that under extending configuration. The above experimental results reveal that the as-fabricated nanosheets-based ECD possesses good cyclic stability and excellent flexibility, which further verifies the structural advantages of ultrathin nanosheets.

Discussion

In summary, large-area nanosheets of tungsten oxide dihydrate with a thickness of only about 1.4 nm are synthesized for the first time via ultrasonic exfoliation of lamellar inorganic–organic hybrid intermediate. Compared with the bulk counterpart, $WO_3 \cdot 2H_2O$ ultrathin nanosheets possess more flexible feature, better interface contact with the substrate and higher Li^+ diffusion coefficients. The as-exfoliated ultrathin nanosheets can be assembled into free-standing thin films using the convenient vacuum filtration, and then the as-assembled film can easily transfer into a flexible substrate for fabricating flexible electrochromic device. The obtained device exhibits

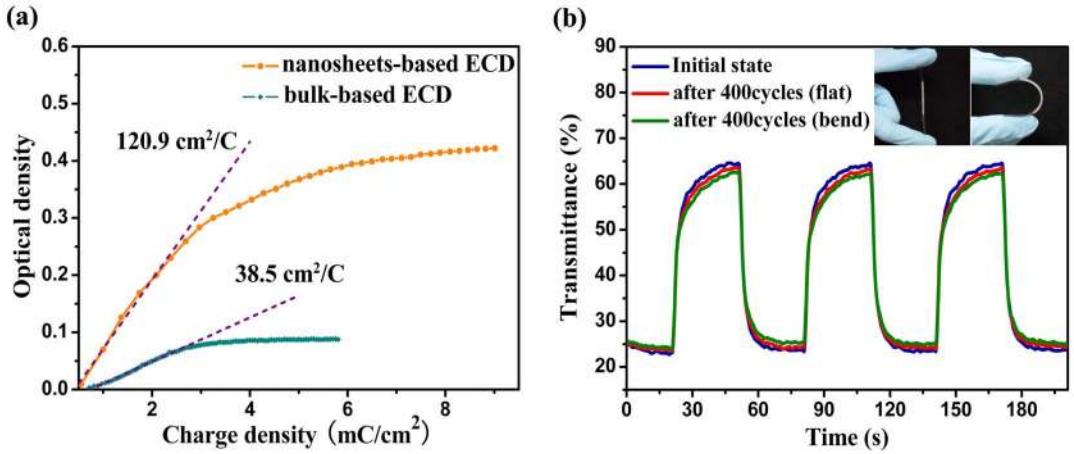

Figure 6 | Coloration efficiency and cyclic stability of $WO_3 \cdot 2H_2O$ nanosheets-based ECD. (a) Variation of the in situ optical density (OD) vs. the charge density (Q/A) for $WO_3 \cdot 2H_2O$ nanosheets-based ECD and the comparative bulk-based ECD recorded at 700 nm. (b) Change in optical transmittance versus time for $WO_3 \cdot 2H_2O$ nanosheets-based ECD at initial cycle (blue), after 400 cycles under extending configuration (red) and after 400 cycles under bending configuration (green).

large transparency contrast, fast coloration/bleaching response speed, high coloration efficiency, good cycling stability and excellent flexibility. These superior electrochromic performances are strikingly higher than those of $WO_3 \cdot 2H_2O$ bulk-based ECD and the previously reported flexible ECDs in full consideration of various parameters, which can be ascribed to the synergetic effect between the unique atomic structure of $WO_3 \cdot 2H_2O$ and the morphological features of ultrathin nanosheets. The calculated density of states for $WO_3 \cdot 2H_2O$ and $Li_xWO_3 \cdot 2H_2O$ indicate that $WO_3 \cdot 2H_2O$ undergoes a transition from semiconducting to metallic state accompanied by Li^+ intercalation, which is the reason of electrochromism. The relationship between the structural features of ultrathin nanosheets and color-switching speed is further researched, and the results manifest that $WO_3 \cdot 2H_2O$ ultrathin nanosheets can effectively facilitate the semiconductor-to-metal transition and increase the coloration/bleaching response speed, especially for the coloration process. It will provide plenty of valuable information for ultrathin 2D nanosheets to develop the high-performance flexible electrochromic devices. The excellent electrochromic performances with the combination of flexibility make our device a prominent candidate in flexible and portable electronics.

Methods

Synthesis of tungstate-based inorganic–organic nanohybrids. The reactions between tungstic acid (H_2WO_4) and dodecylamine ($C_{12}H_{25}NH_2$) were carried out at room temperature according to the reported process, with some modification[53]. Typically, 0.3 g of H_2WO_4 powder was dispersed in a mixture of 3 g of $C_{12}H_{25}NH_2$ and 15 mL of heptane with magnetic stirring. The continuous stirring was maintained for 48 h till the color of reaction system was changed from yellow to white. The samples were centrifuged and washed with ethanol twice. The white solid powder obtained was dried overnight at room temperature.

Exfoliation of tungstate-based inorganic–organic nanohybrids and fabrication of transferrable $WO_3 \cdot 2H_2O$ thin film. In a typical experiment, 45 mg tungstate-based inorganic–organic nanohybrids were dispersed in 45 ml of 4.8 M nitric acid solution. The mixture was stirred for 48 h at 10°C and then ultrasonicated in iced water for 6 hours. A light-yellow suspension was obtained and centrifuged at 2000 rpm for 15 min to remove the nonexfoliated component. Then the obtained supernatant was vacuum-filtrated over a cellulose membrane with 0.22 μm pore size, after which the resulting thin film was washed with deionized water.

Assembly of flexible electrochromic device. Polyethylene terephthalate (PET) coated with indium tin oxide (ITO) was employed as the flexible substrate and was purchased from Sigma Aldrich (45 Ω/sq). For working electrode, a $WO_3 \cdot 2H_2O$ ultrathin nanosheet film with 1.5 cm × 1.5 cm planar size was transferred onto the ITO/PET sheet (for details see supporting information S4 and **Figure S4**). The ECD was fabricated by coating a 1 mm thick adhesive agent on the four sides of the nanosheet film on ITO/PET sheet, and then another ITO/PET sheet as counter electrode was laid on the top of the adhesive agent. Finally, 1 M lithium perchlorate ($LiClO_4$) in propylene carbonate (PC) as the electrolyte was injected into the space between two electrodes, until all air was replaced. The flexible electrochromic device (designated as nanosheets-based ECD) was successfully assembled. For comparison, tungsten oxide dihydrate bulk powder was synthesized using the method of Freedman (see details in S5 and **Figure S5**)[35,54]. The film coated with $WO_3 \cdot 2H_2O$ bulk powder for ECD was prepared by dropping the suspension of $WO_3 \cdot 2H_2O$ powder onto the ITO/PET sheet and then drying at room temperature. Other procedures were the same as those used to fabricate the nanosheets-based ECD. The obtained electrochromic device made of $WO_3 \cdot 2H_2O$ bulk powder was designated as bulk-based ECD.

Characterizations. The samples were characterized using XRD with Philips X'Pert Pro Super diffractometer with Cu-Kα radiation (λ = 1.54178 Å). The transmission electron microscopy (TEM) images and high-resolution TEM (HRTEM) images were performed on a JEOL-2010 transmission electron microscope at an acceleration voltage of 200 kV. Tapping-mode atomic force microscopy (AFM) images were obtained on DI Innova Multimode SPM platform. Cyclic voltammograms were measured using electrochemical station (CHI660B) in a conventional three-electrode cell. The $WO_3 \cdot 2H_2O$ ultrathin nanosheets and bulk powder were deposited on ITO glasses served as the working electrodes, respectively. Pt was used as the counter electrode, Ag/AgCl was the reference electrode and the electrolyte was 1 M $LiClO_4$/PC. The optical transmittance spectra of electrochromic devices were recorded from 350 to 1300 nm using a Perkin-Elmer Lambda 950 UV/Vis-NIR spectrophotometer. The coloration/bleaching switching characteristics of electrochromic device were measured by transmittance variation at a wavelength of 700 nm with alternately applying potential of ± 3.0 V, 30 s for each state.

1. Choy, J. H. *et al.* New solution route to electrochromic poly(acrylic acid)/WO_3 hybrid film. *Chem. Mater.* **12**, 2950-2956 (2000).
2. Santato, C., Odziemkowski, M., Ulmann, M. & Augustynski, J. Crystallographically oriented mesoporous WO_3 films: synthesis, characterization, and applications. *J. Am. Chem. Soc.* **123**, 10639–10649 (2001).
3. Lee, S. H. *et al.* Electrochromic mechanism in a-WO_{3-y} thin films. *Appl. Phys. Lett.* **74**, 242–244 (1999).
4. Niklasson, G. A. & Granqvist, C. G. Electrochromics for smart windows: thin films of tungsten oxide and nickel oxide, and devices based on these. *J. Mater. Chem.* **17**, 127–156 (2007).
5. Mortimer, R. J., Dyer, A. L. & Reynolds, J. R. Electrochromic organic and polymeric materials for display applications. *Displays* **27**, 2–18 (2006).
6. Byker, H. J. Electrochromics and polymers. *Electrochim. Acta* **46**, 2015–2022 (2001).
7. Gillaspie, D. T., Tenent, R. C. & Dillon, A. C. Metal-oxide films for electrochromic applications: present technology and future directions. *J. Mater. Chem.* **20**, 9585–9592 (2010).
8. Lin, Y.-S., Chiang, Y.-L. & Lai, J.-Y. Effects of oxygen addition to the electrochromic properties of WO_{3-z} thin films sputtered on flexible PET/ITO substrates. *Solid State Ionics* **180**, 99–105 (2009).
9. White, C. M., Gillaspie, D. T., Whitney, E., Lee, S. H. & Dillon, A. C. Flexible electrochromic devices based on crystalline WO_3 nanostructures produced with hot-wire chemical vapor deposition. *Thin Solid Films* **517**, 3596–3599 (2009).
10. Bessiere, A. *et al.* Sol–gel deposition of electrochromic WO_3 thin film on flexible ITO/PET substrate. *Electrochim. Acta* **46**, 2251–2256 (2001).

11. Lin, Y. S., Lai, J. Y., Tsai, T. H., Chuang, P. Y. & Chen, Y. C. Effects of oxygen addition on electrochromic properties in low temperature plasma-enhanced chemical vapor deposition-synthesized MoOxCy thin films for flexible electrochromic devices. *Thin Solid Films* **519**, 3875–3882 (2011).
12. Argun, A. A. & Reynolds, J. R. Line patterning for flexible and laterally configured electrochromic devices. *J. Mater. Chem.* **15**, 1793–1800 (2005).
13. Yao, Z., Di, J., Yong, Z., Zhao, Z. & Li, Q. Aligned coaxial tungsten oxide-carbon nanotube sheet: a flexible and gradient electrochromic film. *Chem. Commun.* **48**, 8252–8254 (2012).
14. Ke, L., Kumar, R. S., Chua, S. J. & Burden, A. P. Degradation study in flexible substrate organic light-emitting diodes. *Appl. Phys. A.* **81**, 969–974 (2005).
15. Chen, D. *et al.* The enhanced alcohol-sensing response of ultrathin WO_3 nanoplates. *Nanotechnology* **21**, 035501 (2010).
16. Feng, J. *et al.* Metallic few-layered VS_2 ultrathin nanosheets: high two-dimensional conductivity for in-plane supercapacitors. *J. Am. Chem. Soc.* **133**, 17832–17838 (2011).
17. Xie, J. *et al.* Layer-by-layer b-Ni$(OH)_2$/graphene nanohybrids for ultraflexible all-solid-state thin-film supercapacitors with high electrochemical performance. *Nano Energy* **2**, 65–74 (2013).
18. Feng, J. *et al.* Giant moisture responsiveness of VS_2 ultrathin nanosheets for novel touchless positioning interface. *Adv. Mater.* **24**, 1969–1974 (2012).
19. Sun, Y., Wu, Q. & Shi, G. Graphene based new energy materials. *Energy Environ. Sci.* **4**, 1113–1132 (2011).
20. Zhu, Y. *et al.* Carbon-based supercapacitors produced by activation of graphene. *Science* **332**, 1537–1541 (2011).
21. Meric, I. *et al.* Current saturation in zero-bandgap, topgated graphene field-effect transistors. *Nat. Nanotechnol.* **3**, 654–659 (2008).
22. Sun, Y. *et al.* Fabrication of flexible and freestanding zinc chalcogenide single layers. *Nat. Commun.* **3** (2012).
23. Ma, R. & Sasaki, T. Nanosheets of oxides and hydroxides: ultimate 2D charge-bearing functional crystallites. *Adv. Mater.* **22**, 5082–5104 (2010).
24. Osada, M. & Sasaki, T. Exfoliated oxide nanosheets: new solution to nanoelectronics. *J. Mater. Chem.* **19**, 2503–2511 (2009).
25. Park, S. Y., Lee, J. M., Noh, C. & Son, S. U. Colloidal approach for tungsten oxide nanorod-based electrochromic systems with highly improved response times and color efficiencies. *J. Mater. Chem.* **19**, 7959–7964 (2009).
26. Lee, S. H. *et al.* Crystalline WO_3 nanoparticles for highly improved electrochromic applications. *Adv. Mater.* **18**, 763–766 (2006).
27. Zhang, J. *et al.* Enhanced electrochromic performance of macroporous WO_3 films formed by anodic oxidation of DC-sputtered tungsten layers. *Electrochim. Acta* **55**, 6953–6958 (2010).
28. Bessiere, A. *et al.* Flexible electrochromic reflectance device based on tungsten oxide for infrared emissivity control. *J. Appl. Phys.* **91**, 1589–1594 (2002).
29. Zheng, H. *et al.* Nanostructured tungsten oxide - properties, synthesis, and applications. *Adv. Funct. Mater.* **21**, 2175–2196 (2011).
30. Xie, Z. *et al.* Fast fabrication of $WO_3 \cdot 2H_2O$ thin film with improved electrochromic properties. *J. Mater. Chem.* **22**, 19904–19910 (2012).
31. Wei, X. L. & Shen, P. K. Electrochromics of single crystalline $WO_3 \cdot H_2O$ nanorods *Electrochem. Commun.* **8**, 293–298 (2006).
32. Costa, C., Pinheiro, C., Henriques, I. & Laia, C. A. T. Inkjet printing of sol-gel synthesized hydrated tungsten oxide nanoparticles for flexible electrochromic devices. *ACS Appl. Mater. Interfaces* **4**, 1330–1340 (2012).
33. Judeinstein, P. & Livage, J. Electrochemical mechanisms in tungsten oxide thin films. *J. Chim. Phys.* **90**, 1137–1147 (1993).
34. Marcel, C. & Tarascon, J. M. An all-plastic $WO_3 \cdot H_2O$/polyaniline electrochromic device. *Solid State Ionics* **143**, 89–101 (2001).
35. Li, Y. M., Hibino, M., Miyayania, M. & Kudo, T. Proton conductivity of tungsten trioxide hydrates at intermediate temperature. *Solid State Ionics* **134**, 271–279 (2000).
36. Kattouf, B., Frey, G. L., Siegmann, A. & Ein-Eli, Y. Enhanced reversible electrochromism via in situ phase transformation in tungstate monohydrate. *Chem. Commun.* 7396–7398 (2009).
37. Kalantar-zadeh, K. *et al.* Synthesis of atomically thin WO_3 sheets from hydrated tungsten trioxide. *Chem. Mater.* **22**, 5660–5666 (2010).
38. Sun, Y. *et al.* Freestanding tin disulfide single-layers realizing efficient visible-light water splitting. *Angew. Chem. Int. Ed.* **51**, 8727–8731 (2012).
39. Deliang, C., Lian, G., Yasumori, A., Kuroda, K. & Sugahara, Y. Size- and shape-controlled conversion of tungstate-based inorganic-organic hybrid belts to WO_3 nanoplates with high specific surface areas. *Small* **4**, 1813–1822 (2008).
40. Balaji, S., Djaoued, Y., Albert, A. S., Ferguson, R. Z. & Bruening, R. Hexagonal tungsten oxide based electrochromic devices: spectroscopic evidence for the Li ion occupancy of four-coordinated square windows. *Chem. Mater.* **21**, 1381–1389 (2009).
41. Liao, C. C., Chen, F. R. & Kai, J. J. WO_{3-x} nanowires based electrochromic devices. *Sol. Energy Mater. Sol. Cells* **90**, 1147–1155 (2006).
42. Souza, F. L., Aegerter, M. A. & Leite, E. R. Solid hybrid polyelectrolyte with high performance in electrochromic devices: Electrochemical stability and optical study. *Sol. Energy Mater. Sol. Cells* **91**, 1825–1830 (2007).
43. Jiao, Z., Sun, X. W., Wang, J., Ke, L. & Demir, H. V. Hydrothermally grown nanostructured WO_3 films and their electrochromic characteristics. *J. Phys. D: Appl. Phys.* **43**, 285501 (2010).
44. Gubbala, S., Thangala, J. & Sunkara, M. K. Nanowire-based electrochromic devices. *Sol. Energy Mater. Sol. Cells* **91**, 813–820 (2007).
45. Wang, M. *et al.* High optical switching speed and flexible electrochromic display based on WO_3 nanoparticles with ZnO nanorod arrays' supported electrode. *Nanotechnology* **20**, 185304 (2009).
46. Broclawik, E., Gora, A., Liguzinski, P., Petelenz, P. & Slawik, M. Quantum chemical modelling of the process of lithium insertion into WO_3 films. *Catal. Today* **101**, 155–162 (2005).
47. Granqvist, C. G. Electrochromic tungsten oxide films: review of progress 1993–1998. *Sol. Energy Mater. Sol. Cells* **60**, 201–262 (2000).
48. Green, M. & Pita, K. Non-stoichiometry in thin film dilute tungsten bronzes: M_xWO_{3-y}. *Sol. Energy Mater. Sol. Cells* **43**, 393–411 (1996).
49. Kamal, H., Akl, A. A. & Abdel-Hady, K. Influence of proton insertion on the conductivity, structural and optical properties of amorphous and crystalline electrochromic WO_3 films. *Physica B* **349**, 192–205 (2004).
50. Jiao, Z. *et al.* Electrochromic properties of nanostructured tungsten trioxide (hydrate) films and their applications in a complementary electrochromic device. *Electrochim. Acta* **63**, 153–160 (2012).
51. Mortimer, R. J. Electrochromic Materials. *Annu. Rev. Mater. Res.* **41**, 241–268 (2011).
52. Xiong, C., Aliev, A. E., Gnade, B. & Balkus, K. J. Jr. Fabrication of silver vanadium oxide and V_2O_5 nanowires for electrochromics. *ACS Nano* **2**, 293–301 (2008).
53. Chen, D. *et al.* A comparative study on reactions of n-alkylamines with tungstic acids with various W-O octahedral layers: Novel evidence for the "dissolution-reorganization" mechanism. *Mater. Chem. Phys.* **125**, 838–845 (2011).
54. Freedman, M. L. The tungstic acids. *J. Am. Chem. Soc.* **81**, 3834–3839 (1959).

Acknowledgements

This work was financially supported by National Basic Research Program of China (2009CB939901), the Chinese Academy of Sciences (XDB01020300), and National Nature Science Foundation (11079004).

Author contributions

L.L. and Y.X. conceived the idea and co-wrote the paper. L.L., Y.Y.Z., J.F.X., X.D.Z. and M.L.G. carried out the examples synthesis and characterization. J.J.Z. and B.C.P. carried out the theoretical calculations. All the authors discussed the results, commented on and revised the manuscript.

Additional information

Supplementary information accompanies this paper at http://www.nature.com/scientificreports

Competing financial interests: The authors declare no competing financial interests.

How to cite this article: Liang, L. *et al.* High-performance flexible electrochromic device based on facile semiconductor-to-metal transition realized by $WO_3 \cdot 2H_2O$ ultrathin nanosheets. *Sci. Rep.* **3**, 1936; DOI:10.1038/srep01936 (2013).